Arabian Journal of Geosciences (2020) 13: 43
https://doi.org/10.1007/s12517-019-5043-3

ORIGINAL PAPER

Predicting 3D heterogeneous in situ stress field of Gaoshangpu Oilfield northern area, Nanpu Sag, Bohai Bay Basin, China

Ke Xu[1,2] · Junsheng Dai[1] · Jianwei Feng[2] · Bifeng Wang[2] · Lin Shang[3] · Lu Fang[2] · Shuo Wang[4]

Received: 17 June 2019 / Accepted: 19 December 2019 / Published online: 7 January 2020

Abstract
Research on in situ stress has important theoretical and practical significance for the exploration and development of oil and gas reservoirs. The orientation and magnitude of in situ stress in the Gaoshangpu Oilfield northern area (GO-NA) were analyzed using borehole breakout data and acoustic emission measurements. Mechanical experiments, logging interpretation, and seismic data enabled spatial characterization of rock mechanics parameters. A 3D geological model and 3D heterogeneous rock mechanics field of the GO-NA were constructed. Petrel and ANSYS modeling provided detailed prediction of the 3D stress field in the GO-NA. The results indicate that the maximum horizontal stress orientation in the GO-NA is generally ENE–WSW-trending, with significant changes in in situ stress orientation within and between fault blocks. Along surfaces and profiles, stress magnitudes are discrete and in situ stress is of the Ia-type. Observed inter-strata differences were characterized by five different types of in situ stress profile. Faults are the most important factor in the large distributional differences in the stress field of reservoirs observed within the complex fault blocks, significantly affecting magnitudes and orientations in the stress field. The next most important influence on the stress field is the reservoir's rock mechanics parameters, which affect in situ stress magnitudes. A strong linear correlation exists between reservoir depth and in situ stress magnitude. This technique provides a theoretical basis for more efficient exploration and development of low-permeability reservoirs. It also serves as a reference for the detailed prediction of inter-well in situ stress in regions with similarly complex fault blocks.

Keywords Complex fault blocks · Three-dimensional heterogeneity · In situ stress prediction · Reservoir model · Gaoshangpu Oilfield

Abbreviations

3D	Three-dimensional
FEM	Finite element method
GO-NA	Gaoshangpu Oilfield northern area
GO-SA	Gaoshangpu Oilfield southern area
S_{hmin}	Minimum horizontal stress
S_{Hmax}	Maximum horizontal stress
S_{V}	Vertical stress
FMI	Fullbore Formation Microimager
AE	Acoustic emission

Responsible Editor: François Roure

✉ Ke Xu
xukee0505@163.com

[1] Exploration and Development Research Institute (EDRI), PetroChina Tarim Oilfield Company, No. 26, Shihua Road, Korla 841000, Xinjiang, China

[2] School of Geosciences, China University of Petroleum (Huadong) [CUP(H)], Qingdao 266580, Shandong, China

[3] EDRI, PetroChina Jidong Oilfield Company, Tangshan 063004, Hebei, China

[4] EDRI, PetroChina Xinjiang Oilfield Company, Karamay 834000, Xinjiang, China

Introduction

In situ stress refers to the internal stress within the Earth's crust, and is closely related to gravitational and tectonic stresses (Bell 1996; Kang et al. 2010). Knowledge of the in situ stress field of a reservoir is important in petroleum exploration and field development (Finkbeiner et al. 2001; Bell 2006; Zoback 2007; Tingay et al. 2010; Li et al. 2014; Ju and Sun 2016; Ju et al. 2017), because it can affect permeable fracture aperture and orientation as well as fault sealing. Understanding in situ stress also plays an important role in solving engineering problems, such as underground excavation design (Mizuta et al. 1987), wellbore stability evaluation (Zoback et al. 2003; Tingay et al. 2009), and the optimization of ground support systems (Sibson 1994; Binh et al. 2007; Liu et al. 2016).

In recent years, low-permeability reservoirs have attracted considerable research interest globally due to their potential for oil and gas (Farrell et al. 2014; Lommatzsch et al. 2015; Nelson 2009; Zeng et al. 2013). Fracking is a current trend and an effective method for developing low-permeability reservoirs. During hydraulic fracturing, fracture-form, method of fracture extension, and production efficiency are greatly influenced by the state of the in situ stress field. The four most important research aspects during the development of low-permeability reservoirs are (1) changes in stress within the reservoir; (2) deformation and fracturing mechanisms of the rock; (3) optimization of horizontal well trajectories; and (4) hydraulic fracturing design (He et al. 2015; Hoda et al. 2015). In situ stress is one of the most significant characteristics when assessing these key factors. Comprehensive evaluation of in situ reservoir stress, utilizing various methods, is imperative (Zeng et al. 2013; Zoback et al. 2003).

The most direct and effective means of determining in situ stress are well site measurements and the acquisition of cores data for testing. Core testing includes paleomagnetic orientation, wave velocity anisotropy, acoustic emission, and differential strain; field measurement methods include borehole breakouts, drilling-induced fractures, and downhole microseismic monitoring. These methods can indicate the magnitude and orientation of in situ stress (Dai 2002; Zoback 2007; Zang and Stephansson 2009; Zhang et al. 2012). These techniques are relatively well developed and widely applied. Various models using well logging data have been proposed to calculate the in situ stress of heterogeneous strata (Wang et al. 2008; Chen et al. 2009a; Fan et al. 2009), to obtain one-dimensional and continuous in situ stress data for entire well sections.

There remains a lack of mature analytical methods and techniques for predicting the distribution of inter-well in situ stress, especially in regions with complex fault blocks and highly heterogeneous stress fields. At present, the main methods for predicting in situ stress fields are two-dimensional or three-dimensional (3D) numerical simulations using the finite element method (FEM) and wells as constraints (Xie et al. 2008; Liu et al. 2009; Tian et al. 2011; Yang et al. 2012; Yu et al. 2016; Dai et al. 2016). The former is mainly used for large-scale basin modeling. It focuses on predicting in situ stress orientation and qualitative to semi-quantitative studies of in situ stress magnitudes. The latter can reflect the distribution of the stress field within target strata in 3D space. However, prediction accuracies are largely dependent on the construction of the geological model and determination of the rock mechanics parameters.

Previous studies have applied digital processing to the target layers in a tectonic map to obtain the 3D coordinates of the layers (Wang et al. 2007; Dai et al. 2011, 2014; Ding et al. 2011, 2016; Lei et al. 2015; Wang et al. 2016). However, the precision of digitization is low, resulting in oversimplification of faults. Furthermore, the mechanical models used are stratified horizontally and have homogeneous planes, meaning that well-constrained rock mechanics parameters are substituted for those of a particular area or entire region (Zhu et al. 2016). Such approaches do not meet the requirements for understanding the in situ stress field of reservoirs within complex fault blocks.

This study examines a deep-buried reservoir in the Gaoshangpu Oilfield northern area (GO-NA). Research on in situ stress of the GO-NA can provide technical support for well-planning and the design of fracturing schemes (Cao 2005; Haghi et al. 2013), thereby potentially improving the outcomes of reservoir exploration and development.

In view of the aforementioned issues, the enhanced method proposed here employs two innovations: (i) seamlessly joining geological and FEM models, using a combined Petrel and ANSYS modeling technique to more accurately model the actual undulations of target strata in the study area and produce detailed 3D fault characterizations; and (ii) using a combination of core tests and geophysical methods to construct a 3D heterogeneous rock mechanics model of the target strata. These will be used to predict in situ stress distributions in the GO-NA field and to inform optimum well pattern design within the strata for fracturing.

Overview of study area

Bohai Bay Basin is an important hydrocarbon-producing province on the eastern coast of China, covering approximately 200,000 km^2. It appears as a northeast-trending “lazy-Z” pattern (Mann et al. 1983) on the regional geologic map (Dong et al. 2010) (Fig. 1a) and consists of six major depressions: Liaohe, Bozhong, Jiyang, Jizhong, Huanghua, and Linqing (Gong 1997) (Fig. 1b). The deep sandstone reservoir examined here is sited within a region of complex fault blocks formed by the Gaoliu Fault and its derivative faults (Zhang 2010). It is sited in the northern region of the Nanpu Sag, in the northeast part of Huanghua Depression, and covers an area of 1930 km^2. The main oil and gas reservoir is located in the second and third sub-section of the third section of Shahejie Formation (Es_3^{2+3} layer). The Gaoshangpu Oilfield is divided into northern (GO-NA) and southern (GO-SA) areas by the Gaobei Fault. In the GO-SA, NE–SW and NW–SE-striking faults developed in a reticulate pattern, dividing the area into multiple fault blocks that are nearly rectangular or rhombic in shape. The GO-NA is dominated by NE–SW striking faults that divide it into several NE–SW-oriented elongate fault

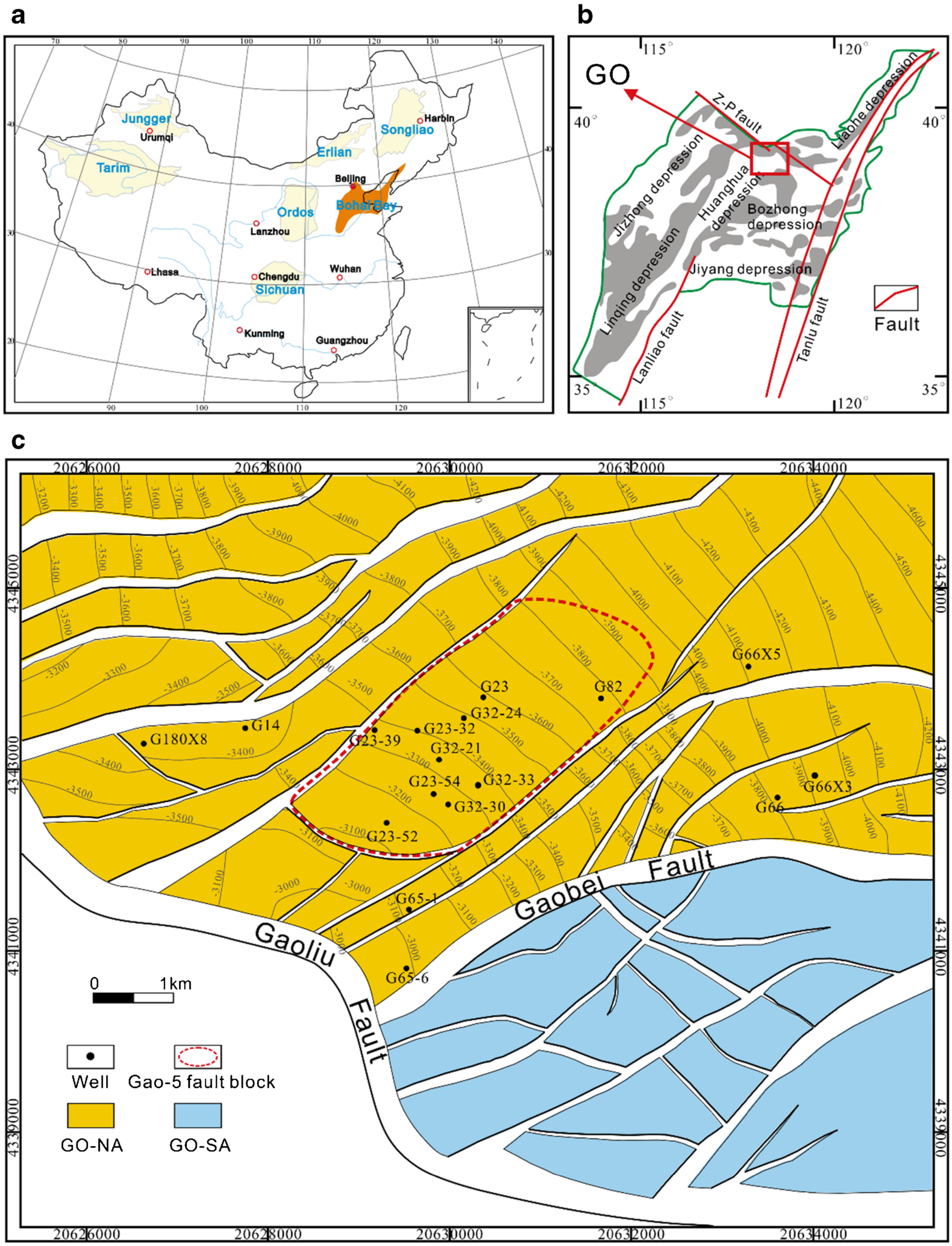

Fig. 1 **a** Map showing the outline of Bohai Basin. **b** Map of Bohai Basin showing the major faults and location of the study area. **c** Map of the study area showing the fault block structure of the GO-NA and Go-SA areas. Contours represent the top surface of Es3^{2+3}

blocks (Fig. 1c). Approximately 70% of the reservoir is oil-bearing and under exploitation (unpublished data from the PetroChina Jidong Oilfield Company 2017). In the middle section of the reservoir is the Gao-5 fault block, which is currently the main focus for exploration and development in the Jidong Oilfield. The target area of this study is the GO-NA's Es_3^{2+3} layer.

Layer Es_3^{2+3} of the GO-NA contains five oil series, labeled I–V from top to bottom (unpublished data from the PetroChina Jidong Oilfield Company 2017). The target layer is buried at a depth of 3000–4000 m and comprises mainly distributary channel sand bodies of subaqueous fan deltas, characterized by highly variable lithofacies and variable fluid properties. Average porosity and permeability are 15.7% and 6.59 mD, respectively, giving the reservoir medium/low porosity and low permeability. In addition, the GO-NA has poor physical properties, high heterogeneity, and minor tectonic fracture growth. The GO-NA is a significant but difficult exploration area within the Jidong Oilfield (Wan et al. 2015). This region of the Jidong Oilfield is currently the focus of exploration and development; however, progress has generally been slow and inefficient due to the poor geological conditions and inadequate exploitation techniques. After many years of waterflooding operations, the oilfield is currently undergoing reassessment for the development of well patterns (unpublished data from the PetroChina Jidong Oilfield Company 2017).

Methodology and input data

In situ stress tensor

In general, the in situ stress state can be described by the stress tensor, which includes the orientation and magnitude of the three orthogonal principal stresses (Engelder 1993). In general, three types of in situ stress regime are determined based on the relative magnitude of the minimum horizontal stress (S_{hmin}), maximum horizontal stress (S_{Hmax}), and vertical stress (S_{V}) (Anderson 1951):

(i) Normal faulting stress regime: $S_{\mathrm{V}} > S_{\mathrm{Hmax}} > S_{\mathrm{hmin}}$: I-type (Ia-type if $S_{\mathrm{hmin}} > 0$; Ib-type if $S_{\mathrm{hmin}} < 0$).
(ii) Strike-slip faulting stress regime: $S_{\mathrm{Hmax}} > S_{\mathrm{V}} > S_{\mathrm{hmin}}$.
(iii) Reverse-faulting stress regime: $S_{\mathrm{Hmax}} > S_{\mathrm{hmin}} > S_{\mathrm{V}}$.

Stress coefficients are important for describing in situ stress and include the ratio between S_{Hmax} and S_{hmin} ($k_{H/h}$), lateral pressure coefficient (k), and S_{Hmax} and S_{hmin} horizontal stress coefficients (k_H and k_h, respectively) (Brown and Hoek 1978; Savage et al. 1992; Engelder 1993; Tingay et al. 2010). Equation 1 can be used to calculate the relationship between the various stress coefficients:

$$\begin{cases} k_{H/h} = S_{\mathrm{Hmax}}/S_{\mathrm{hmin}} \\ k = (S_{\mathrm{Hmax}} + S_{\mathrm{hmin}})/(2S_V) \\ k_H = S_{\mathrm{Hmax}}/S_V \\ k_h = S_{\mathrm{hmin}}/S_V \end{cases} \quad (1)$$

The stability of the reservoir rock is affected by $k_{H/h}$, which is similar to the horizontal differential stress ($S_{\mathrm{Hmax}} - S_{\mathrm{hmin}}$). The larger the ratio, the more unstable the rock (Li et al. 2011b). This causes fractures to extend along the orientation of S_{Hmax}, such that it would be difficult for complex reticulated fractures to form. Coefficient k describes the horizontal stress being borne by the underground rock mass, and is the direct manifestation of the horizontal load at the borehole wall. k_H and k_h describe the relationship between the horizontal and vertical stresses. The stress coefficients and depth cross-plots show a general trend for horizontal in situ stress to increase with depth. This provides supplementary information on the spatial distribution of in situ stress, and reference values for estimating in situ stress in regions lacking such data.

Characteristics of in situ stress at key wells

Orientation of in situ stress by borehole breakouts

Practical experience has shown that the direction of in situ stress can be determined according to the orientation of borehole breakouts (Bell and Gough 1979; Dai 2002; Zoback et al. 2003). When a well is drilled, the removal of rock from the subsurface reduces support of the surrounding rock, resulting in concentrated stresses (Plumb and Hickman 1985; Rajabi et al. 2010). Borehole breakouts occur when the stress exceeds that required to cause rock failure, with the orientation of the borehole breakouts representing the orientation of the minimum horizontal stress (S_{hmin}) (Bell and Gough 1979; Zoback et al. 2003; Brooke-Barnett et al. 2015; Fig. 2a). Generally, borehole breakouts appear in image logs as broad, parallel, and often poorly resolved conductive zones separated by 180°, with caliper enlargement in the direction of the conductive zones (Bell 1996; Rajabi et al. 2010; Tingay et al. 2010; Kingdon et al. 2016). For example, the Fullbore Formation Microimager (FMI) log of an interval of borehole breakout in well G32-21 (Fig. 2a) shows breakout orientation as N–S, indicating that the maximum horizontal stress (S_{Hmax}) was in an E–W orientation. After determining the orientations of borehole breakouts for nine wells, the S_{Hmax} of the GO-NA was determined to be between ENE–WSW and E–W (Fig. 2b and Fig. 8). The image logs and data were obtained from Jidong Oil Company reports.

In situ stress magnitude by acoustic emission

The acoustic emission method is generally used to determine paleo-tectonic stresses experienced in rocks, and can also be used to acquire in situ stress magnitude (Holcomb 1993; Chen et al. 2009b; Li et al. 2011a; Lehtonen et al. 2012; Zhao et al. 2012). Brittle materials retain memories of the loading effect that they have been subjected to (Zang and Stephansson 2009). The stress history of rock can be analyzed based on this characteristic on the basis

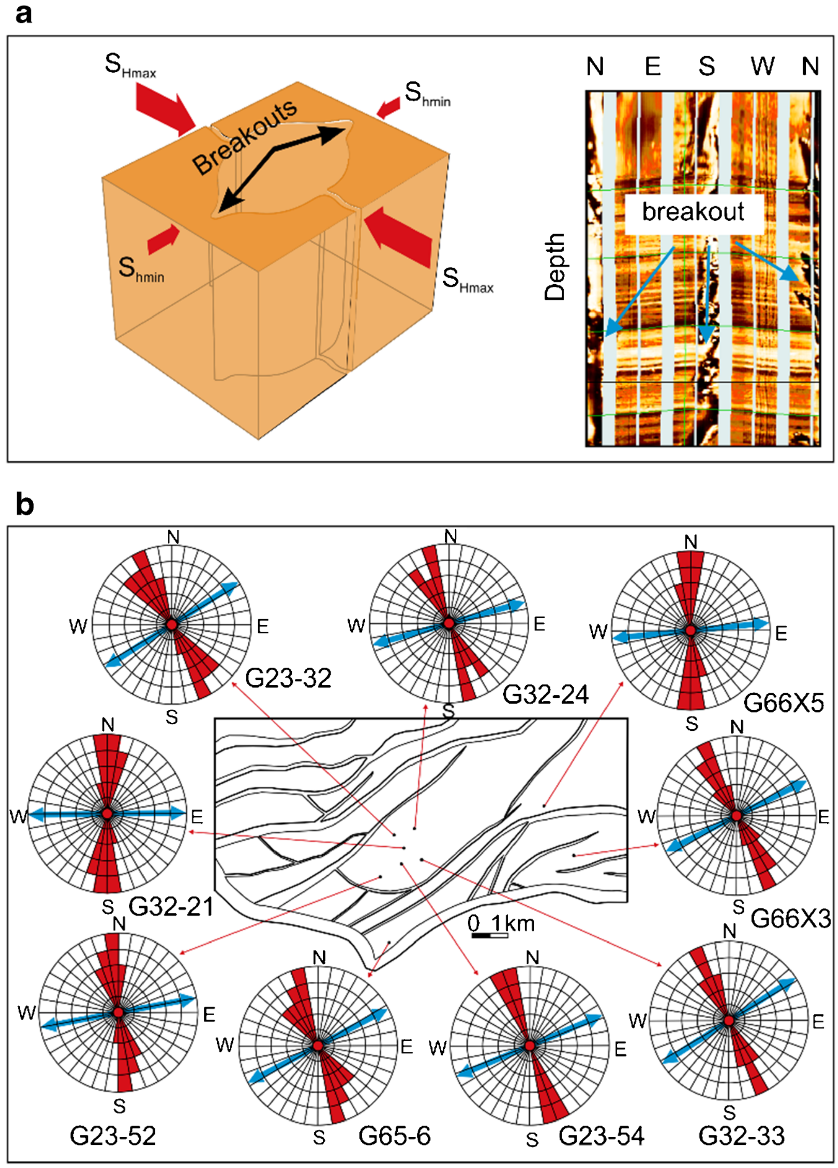

Fig. 2 **a** Borehole breakout as observed in (left) schematic borehole and (right) image logs (example from well G32-21). **b** The azimuth histograms show the orientation of borehole breakouts and the blue arrows indicate S_{Hmax} orientation

of this ability. According to the definition of Kaiser effect, the preexisting maximum stress of sampling point is measured by AE method instead of the current stress. However, after a lot of practice, the concept of "visual Kaiser effect" was proposed. In detail, AE method/curve can obtain two Kaiser points, one corresponding to the stress causing the saturated saturation of the rock. It is consistent with the current stress field and lower than the historical maximum stress value, so it is called the visual Kaiser point. On AE curve, after the visual aiser point, another true Kaiser point is obtained, which corresponds to the highest historical stress.

From above, the load stress experienced by rock samples from different directions (*X*, *Y*, *XY*, and *Z* directions) can be evaluated (Fig. 3), and the values of in situ stress analyzed using the following equations.

$$\begin{cases} \sigma_V = \sigma_\perp \\ \sigma_H = \dfrac{\sigma_x + \sigma_y}{2} + \sqrt{\left(\dfrac{\sigma_x - \sigma_y}{2}\right)^2 + \left(\sigma_{x45y} - \dfrac{\sigma_x + \sigma_y}{2}\right)^2} \\ \sigma_h = \dfrac{\sigma_x + \sigma_y}{2} - \sqrt{\left(\dfrac{\sigma_x - \sigma_y}{2}\right)^2 + \left(\sigma_{x45y} - \dfrac{\sigma_x + \sigma_y}{2}\right)^2} \end{cases} \quad (2)$$

Here, $\sigma_\perp$, σ_x, σ_{x45y}, and σ_y are the in situ stress components of the *Z*, *X*, *XY*, and *Y* directions, respectively.

In this study, 11 groups of AE tests were conducted at Shandong University of Science and Technology (see Table 1). In situ stress magnitude in the GO-NA varies widely: S_{Hmax} and S_{hmin} were 58.20–82.38 MPa and 49.88–72.34 MPa, respectively; S_{V} and horizontal differential stress were 66.15–91.70 MPa and 5.52–13.14 MPa, respectively.

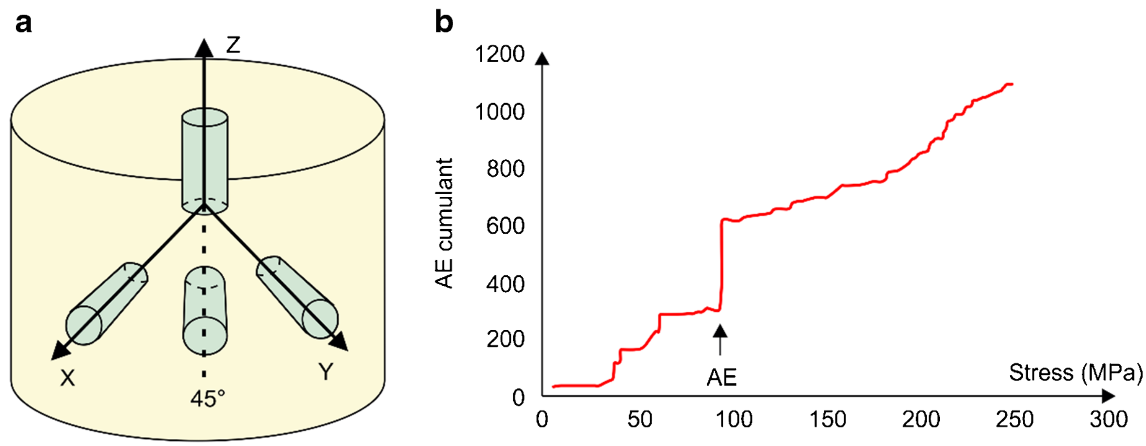

Fig. 3 **a** Sampling acoustic emissions from various directions (*X*, *Y*, *XY*, and *Z* directions). **b** Cumulative acoustic emission graph used to determine magnitude of in situ stress (example from *Y* direction in well G66X5, where stress at point AE = 93.02 MPa)

The overall distribution of in situ stress tended to be lower in the west and higher in the east.

Detailed prediction of a 3D heterogeneous stress field

Figure 3 outlines the workflow involved in detailed prediction of a 3D heterogeneous stress field. First, Petrel 3D visualization software was used to construct a 3D geological model of the target layer in the study area, based on drilling, logging, seismic, and regional geological data. After deriving surface and fault data for the target stratum, AutoCAD software was used to extract the curved surfaces and lines and for model reconstruction. A standalone application was developed to convert the model into a format (iges) recognized by ANSYS software, thereby enabling the model to be imported into ANSYS.

The results of rock mechanics experiments were used as constraints, and were combined with geophysical methods to construct a field model of 3D rock mechanics. The 3D heterogeneous rock mechanics parameters were then assigned to each grid of the FEM model by programming (Fig. 4). The test results for in situ stress in key wells were used as constraints, combined with the geotectonic setting of the study area to determine the appropriate constraints, and then loaded for application to the model. The results were automatically calculated in ANSYS. By seamlessly combining the geological and FEM models, the stress field predictions obtained via numerical simulation were treated as a type of geological information and were again input into the 3D geological model. This allowed the predicted stress fields to be analyzed.

Geological modeling and rock mechanics field

The geological model consists of the structural model, its attributes, and related geological information; the structural

Table 1 Error analysis of simulated in situ stress

Well number	S_{Hmax} (MPa)			S_{hmin} (MPa)			S_V (MPa)			$S_{Hmax} - S_{hmin}$ (MPa)		
	M	S	E	M	S	E	M	S	E	M	S	E
G14	58.20	57.00	1.20	49.88	50.00	0.12	66.15	67.00	0.85	8.32	7.00	1.32
G23	69.50	70.00	0.50	59.46	57.00	2.46	81.05	80.00	1.05	10.04	13.00	2.96
G82	79.37	74.00	5.37	68.28	58.00	10.28	90.23	82.00	8.23	11.09	16.00	4.91
G23-39	72.26	68.00	4.26	59.12	55.00	4.12	88.65	82.00	6.65	13.14	13.00	0.14
G32-30	65.63	66.00	0.37	60.12	55.00	5.12	78.87	73.00	5.87	5.52	11.00	5.48
G66 × 3	81.30	77.00	4.30	70.13	58.00	12.13	86.80	89.00	2.20	11.17	19.00	7.83
G66 × 5	82.38	78.00	4.38	72.34	60.00	12.34	91.70	95.00	3.30	10.04	18.00	7.96
G65-1	62.91	63.00	0.09	54.16	54.00	0.16	70.50	68.00	2.50	8.75	9.00	0.25
G66	78.34	74.00	4.34	67.38	58.00	9.38	86.20	87.00	0.80	10.96	16.00	5.04
G32-21	63.07	67.00	3.93	54.00	56.00	2.00	75.00	73.00	2.00	9.07	11.00	1.93
G180X8	72.00	70.00	2.00	59.50	56.00	3.50	78.60	73.00	5.60	12.50	14.00	1.50

M measured, *S* simulation, *E* error

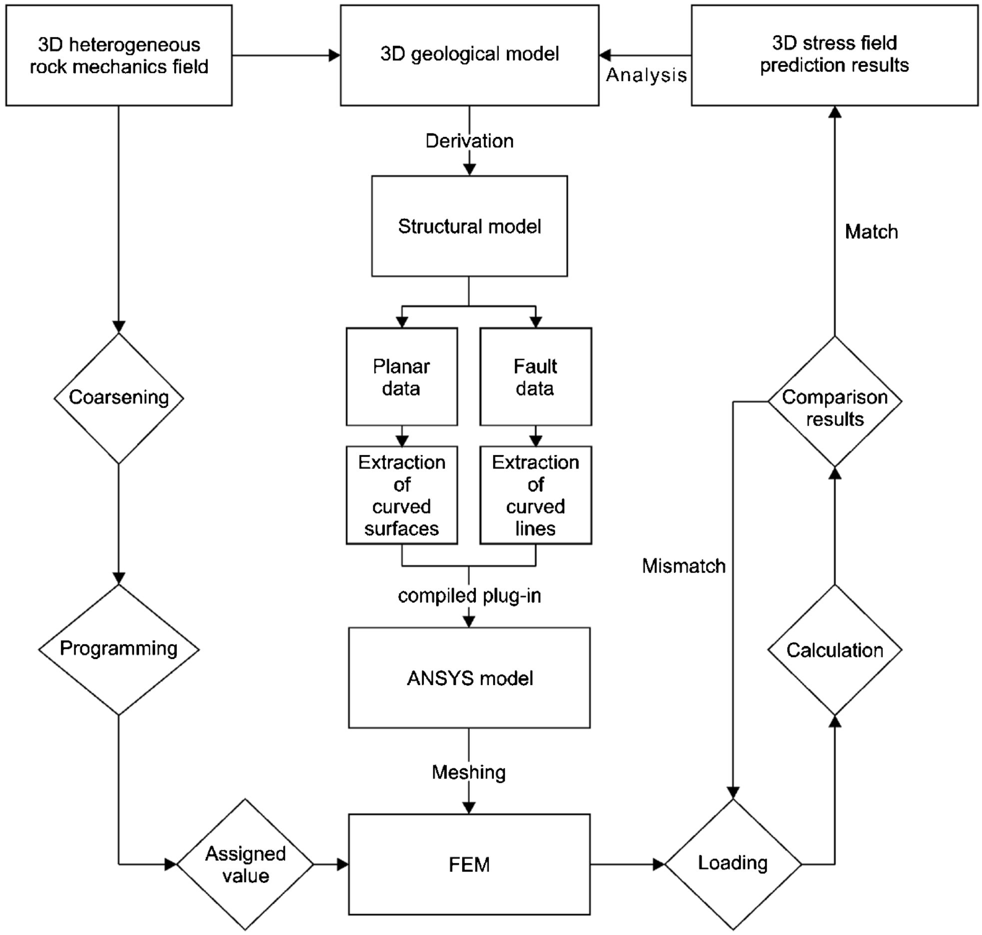

Fig. 4 Flow chart for detailed prediction of 3D heterogeneous stress field

model includes the surface and fault models. The current 3D structural model of the GO-NA comprises 14 faults and the surfaces of five oil series. The area is a monoclinic structure that dips to the north and is divided into multiple fault blocks. The faults are of various sizes, with fault spacings of approximately 20–100 m and dip magnitudes that generally exceed 60°. All are normal faults (Fig. 6a).

The rock mechanics parameters include Young's elastic modulus, Poisson's ratio, and rock density, all of which are prerequisites for in situ stress research. Logging data were used to explain the continuous rock mechanics parameters of a single well profile, calculated as follows (Wang et al. 2014; Lu et al. 2015):

$$E_d = \frac{\rho_b}{\Delta t_s^2} \cdot \frac{3\Delta t_s^2 - 4\Delta t_p^2}{\Delta t_s^2 - \Delta t_p^2} \quad (3)$$

$$\mu_d = \frac{\Delta t_s^2 - 2\Delta t_p^2}{2\left(\Delta t_s^2 - \Delta t_p^2\right)} \quad (4)$$

where E is Young's elastic modulus, MPa; μ is Poisson's ratio, dimensionless; ρ_b is rock density, kg/m^3; and Δt_p and Δt_s are the time differences of the longitudinal and transverse waves, respectively, µs/ft.

The parameters for elasticity calculated from logging data are dynamic, and vary to some extent from the static parameters for elasticity. Since the latter are more suitable for petroleum engineering projects, a conversion relationship was established as a dynamic–static parameter correction (Fig. 5). Static parameters were obtained from rock mechanics experiments. Correction for rock density was not required because this is less affected by experimental and calculation methods.

The 3D distributions of GO-NA rock mechanics parameters were obtained after integrating the area's seismic attributes (Fig. 6). The elastic modulus mainly varied between 24 and 42 GPa, and Poisson's ratio was concentrated at 0.2–0.27. In the 3D space, rock density ranged between 2.05 and 2.60 g/cm^3. The results show clear differences in rock mechanics parameters within and between fault blocks.

Since samples from the GO-NA presented brittle deformation characteristics, numerical simulations and calculations were made according to elastomer data. Solid185 is a high-order, 3D, 20-node solid structural unit in ANSYS that can

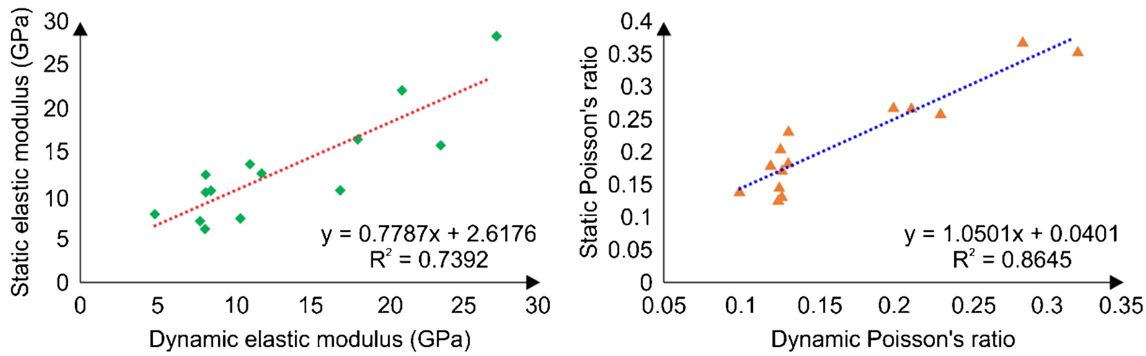

Fig. 5 Linear regression models used as dynamic–static correction parameters for elastic modulus and Poisson's ratio

better simulate irregular grid models and comply with the mechanical characteristics of reservoir rocks (Wang 2014). Hence, it was used as the unit type for faults and strata. After accounting for simulation accuracy and the computational efficiency of the model, the step size of the fault grid and the strata with its surrounding rocks were set to 300 and 500, respectively. The model was divided into 224,528 nodes and 1,323,943 units.

Boundary conditions

Boundary conditions affect the accuracy of the numerically simulated stress fields. Based on the results from the "In situ stress tensor" section, the principal compressive stress in the study area was taken to be orientated ENE. As such, the length of the external frame for the rocks surrounding the model was aligned parallel to that orientation. Next, the geotectonic setting of the study area (Fig. 7b) was considered, using the measured data (Table 1) as constraints.

First, an initial value (uniform pressure of 85, 80, and 90 MPa were applied to the northern, southern, and eastern boundaries, respectively) is set according to the in situ stress value of the key wells. In order to minimize the error between simulated and measured in situ stresses of key wells, following multiple trial calculations and appropriate boundary conditions were ascertained for the model. A pressure of 85 MPa was applied to the western boundary, and pressure gradients of 75–80, 72–80, and 88–93 MPa were applied to the northern, southern, and eastern boundaries, respectively (Fig. 7c). Concurrently, a right-lateral strike-slip of 10 MPa was applied to simulate the impact of the Tanlu fault zone. Another 30 MPa of

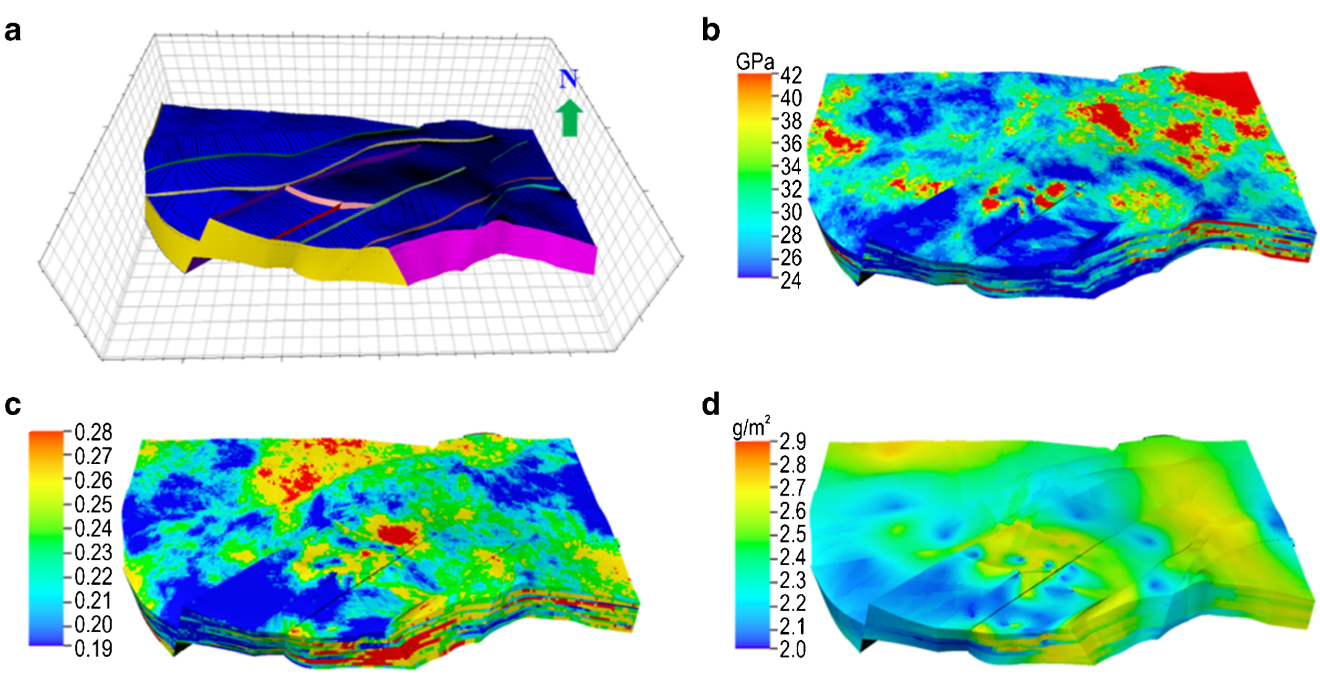

Fig. 6 Structural models of GO-NA and its 3D rock mechanics parameters. **a** 3D geological model of GO-NA. **b** Elastic modulus model. **c** Poisson's ratio model. **d** Rock density model

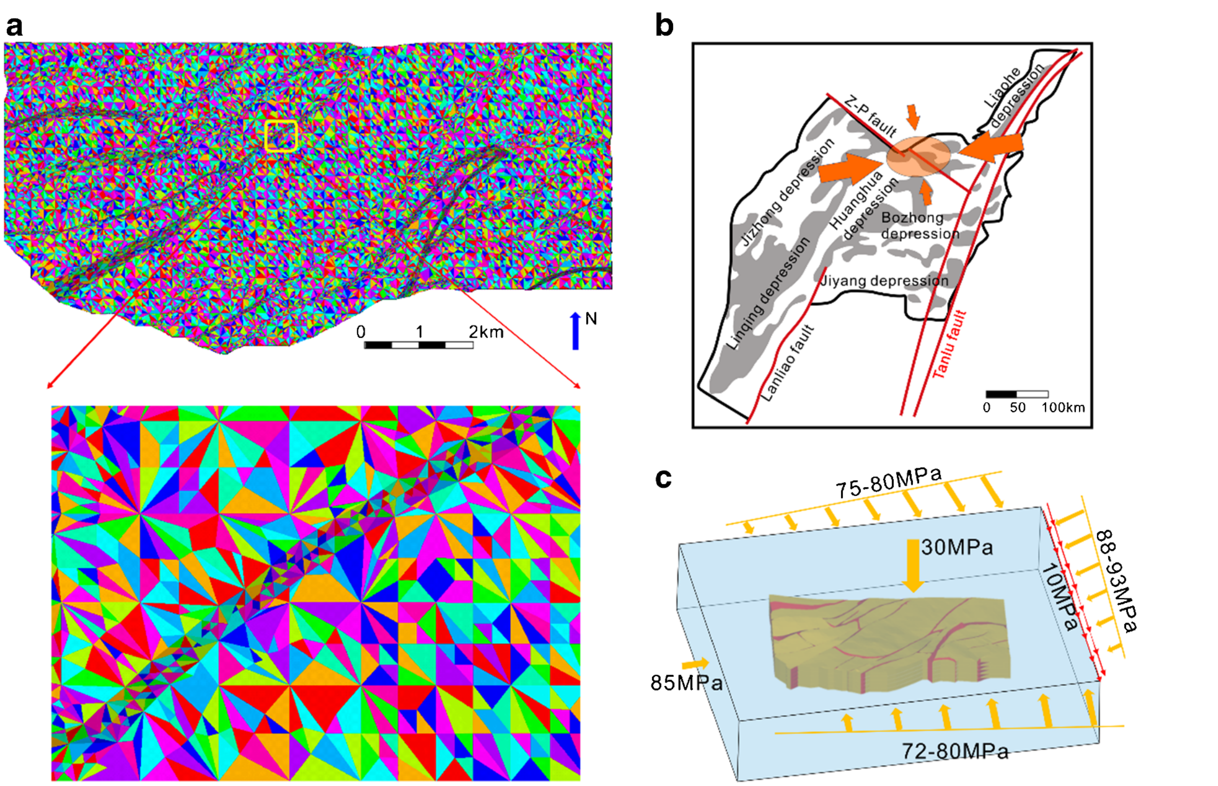

Fig. 7 **a** Mechanical elements of 3D stress fields in adjacent elements, where colors represent different mechanical attributes. **b** Geotectonic background. **c** Setting of boundary conditions

pressure was applied in the downward vertical direction, based on rock mass gravity.

Results and discussion

The distributional characteristics of GO-NA in situ stress were obtained using FEM simulations and calculations. These included the orientations and magnitudes of S_{Hmax}, S_{hmin}, S_V and, horizontal differential stress ($S_{Hmax} - S_{hmin}$). The simulated and measured data were then compared (Fig. 8, Table 1). The average errors in S_{Hmax} and S_{hmin} were 2.79 and 5.60 MPa, respectively, and those for the S_V and horizontal differential stress were 3.55 and 3.58 MPa, respectively.

Distribution of in situ stress orientations

The overall orientation of S_{Hmax} was NE–SW to ENE–WSW with a measured range of 58–238° to 86–266°. In the central region of the study area, the orientation of S_{Hmax} was closer to ENE–WSW, ranging between 68–248° and 72–252°. Orientations in the eastern and western regions gradually rotated toward NE–SW (60–240°; Fig. 7). The orientations of S_{hmin} and S_{Hmax} were perpendicular, and the overall S_{hmin} orientations were NNW–SSE to NW–SE.

Within a fault block, the orientation of S_{Hmax} was relatively uniform and the variations consistent. In contrast, changes in orientation were most obvious between different fault blocks. Studies have shown that lithologic changes can lead to the deflection of stress direction, and there is a quantitative relationship between the mechanical parameters of different lithofacies and the deflection in the direction of in situ stress (Xu et al. 2019). The lithofacies in the study area varies greatly (Fig.6), so it is considered that the non-uniform stress orientations were mainly caused by lithofacies heterogeneity and fault distribution. It caused small but consistent changes in the stress orientation within a fault block. But the faults caused obvious deflections of the stress orientation. Consequently, there were large differences in stress orientation between fault blocks on either side of a fault.

The degree of stress deflection is related to the fault characteristics, including scale (mainly the fault's slip), strike, filling material, and morphology. The angle between fault strike and regional principal stress was the main determinant of deflections in the in situ stress field. The largest deflection angle of S_{Hmax} was observed when fault strike and regional S_{Hmax} formed angles of 30–60°. The deflection was also oriented toward that of the fault. F1 and F2 are boundary faults of the Gao-5 fault block that strike approximately NE–SW (45–225° to 50–230°; Fig. 7). Since the regional S_{Hmax} was oriented ENE–WSW (80–260°), it formed an angle with the two faults

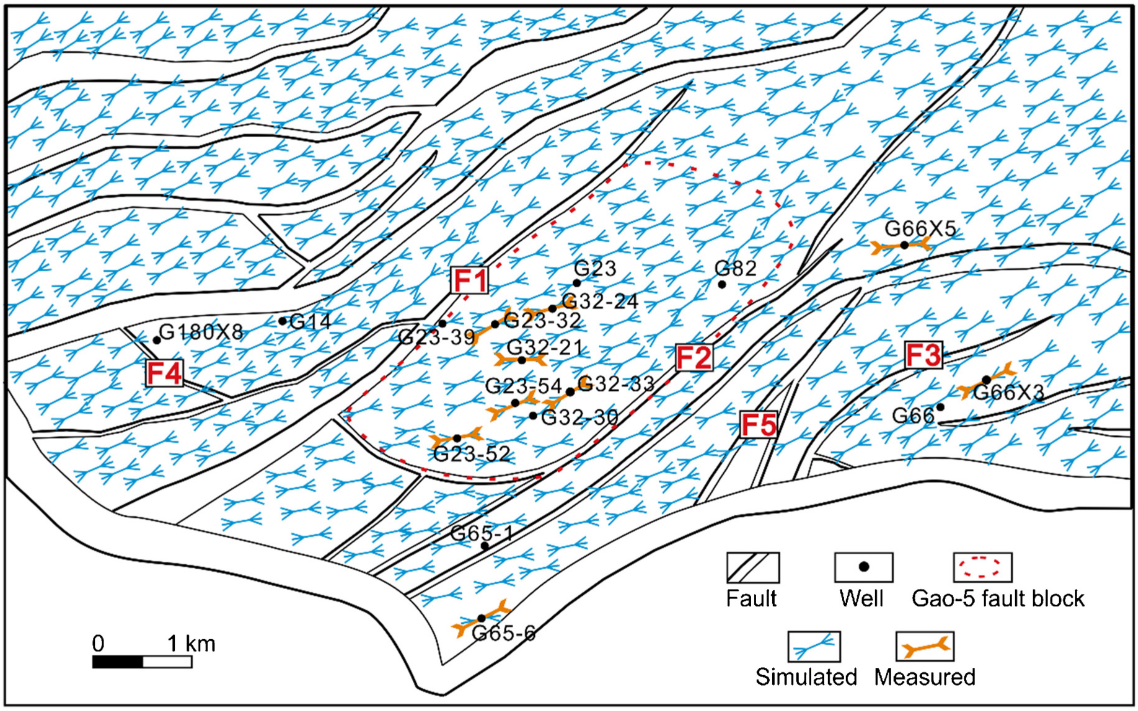

Fig. 8 Measured and simulated orientation of S_{Hmax} in GO-NA

of approximately 35°. Hence, the orientation of S_{Hmax} was deflected along the fault in the vicinity of faults F1 and F2.

When the regional S_{Hmax} and a fault's strike were nearly parallel or perpendicular (i.e., the angle between them was either < 30° or > 60°), S_{Hmax} showed either very small deflection or none. The strike of fault F3 was NE–SW (60–240°), forming an angle of approximately 10° to S_{Hmax}, and the strike of fault F4 was nearly perpendicular (Fig. 6). Thus, near these two faults, there was no obvious deflection in the orientation of S_{Hmax}.

The influence of fault scale on in situ stress was manifested in terms of the magnitude of the fault's slip: larger slip was associated with larger deflection of in situ stress orientation and a wider range of impact; smaller slip was associated with smaller deflection angle and narrower range of impact. As shown in Fig. 8, the deflection of S_{Hmax} caused by fault F5 was less significant than that caused by faults F1 and F2.

Deflection of in situ stress orientation is also affected by the properties of the filling material within a fault zone. Hudson and Cooling (1988) proposed that if the elastic modulus of the filling materials within a fault was lower than that of the surrounding rocks, then stress orientation would be deflected along the fault's strike; if the elastic modulus was higher, stress orientation would be deflected perpendicular to the fault's strike; if both had similar elastic modulus, there would be no deflection. All the faults developed in the GO-NA are of normal type. Interpretation of the core observations and well logging data indicate that the filling materials within the faults had a compaction effect but did not strongly crush the rock mass. In the present case, we can infer that the surrounding rocks have higher elastic modulus, the influence of filling material deflects S_{Hmax} along the fault strike.

In situ stress magnitude

The simulated GO-NA 3D stress fields indicate that the magnitude of S_{Hmax} generally tends to be lower in the west and higher in the east, consistent with the trend observed in measured data. S_{Hmax} mostly ranged between 60 and 85 MPa. Moving from oil series I to oil series V, the magnitude of S_{Hmax} increased with depth. The average stress gradient was 2.08 MPa/100 m. At fault peripheries, stresses were lower, at approximately 57.5–62 MPa (such as F1 in oil series I in Fig. 9a), and S_{Hmax} was reduced by 30% compared with that of the respective layer. Where fault scale was large (wide slip and long extension, such as F1 and F2), it resulted in a larger range in low-magnitude zones. At fault intersections, the internal rock mass was more severely crushed (Xu 2019) and there was greater reduction in stress magnitude. Faults with different dip had different influence on in situ stress distribution: the steeper the fault dip, the smaller the range in low-magnitude zones; the shallower the dip, the larger the range in low-magnitude zones (Table 2).

The magnitude of S_{hmin} showed similar distribution trend to that of S_{Hmax}, being lower in the west and higher in the east. The magnitudes were mainly 50–70 MPa, and average stress gradient was 1.67 MPa/100 m. S_V was approximately 65–98 MPa, and the average stress gradient was 2.25 MPa/

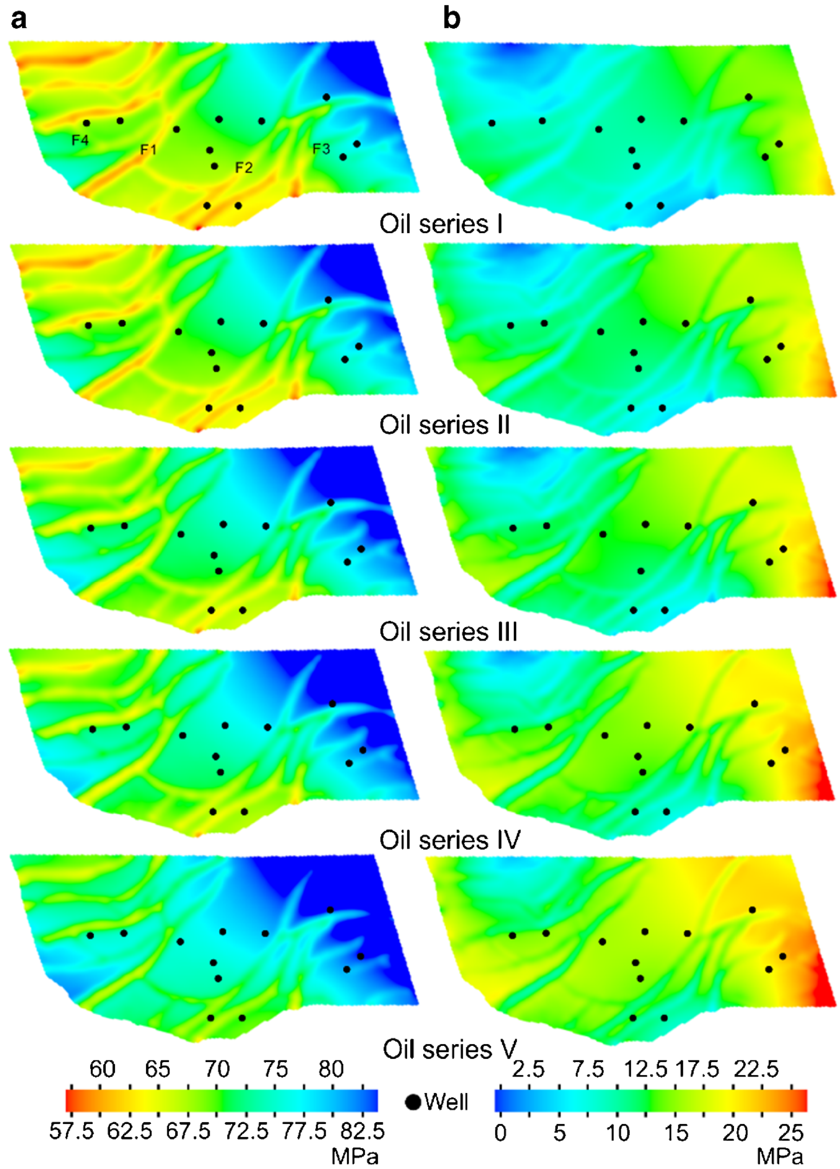

Fig. 9 Simulated GO-NA stress fields for oil series strata I–V. (a) Simulated S_{Hmax}. (b) Simulated horizontal differential stress

100 m (Fig. 10a). Overall, horizontal differential stress was generally < 15 MPa and did not exceed 30 MPa. Again, the spatial distribution showed lower magnitude in the west and higher in the east (Fig. 9b). Within the target layer, in situ stress was categorized as Ia-type ($S_V > S_{Hmax} > S_{Hmin}$) (Anderson 1951).

Table 2 Information of main fault geometry

Fault	Strike	Dip	Length	Distance
F1	NE38~42°	58~64°	9.4 km	120~400 m
F2	NE36~40°	54~60°	8.2 km	100~130 m
F3	NE20~30°	40~45°	3.8 km	120~140 m
F4	NE18~23°	60~66°	2.2 km	80~100 m
F5	NE50~54°	37~45°	3.4 km	100~110 m

Depth data showed ideal linear relationships with S_{Hmax}, S_{hmin}, and S_V (Fig. 10a). Since *S*v is basically related to burial depth and rock density, these parameters showed the highest correlation coefficient (> 0.97). Horizontal stresses were affected by multiple factors, including structural form, strata heterogeneity, and residual tectonic stress. Thus, compared with vertical stress, horizontal stresses showed greater heterogeneity, with correlation coefficient of approximately 0.75. The heterogeneity of the principal stress gradually decreased with increasing depth. For the target GO-NA layer, the S_{Hmax} and S_{hmin} coefficients were concentrated at 0.83 and 0.64, respectively; that of the lateral pressure coefficient was concentrated at 0.74 (Fig. 10b).

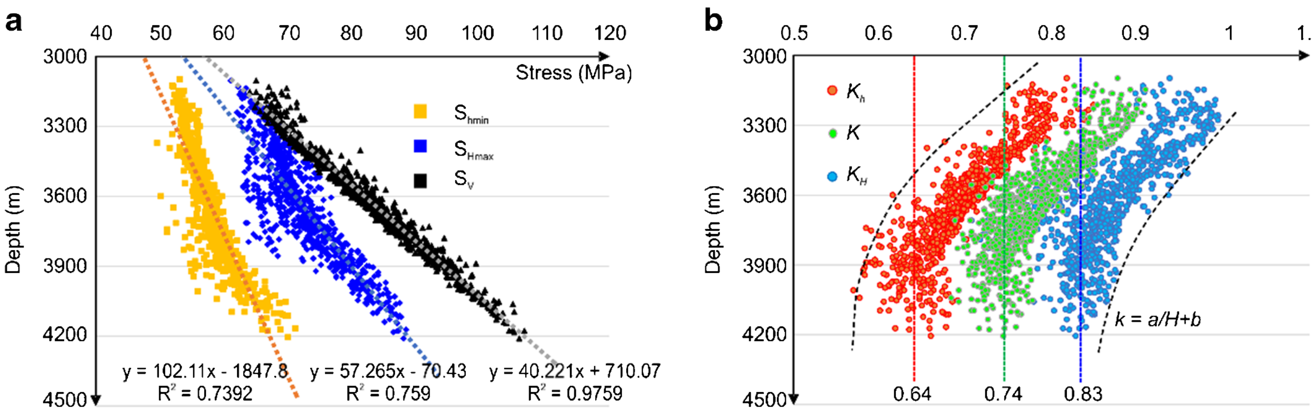

Fig. 10 **a** Relationship between depth and GO-NA principal stress components. **b** Relationship between depth and GO-NA stress coefficients

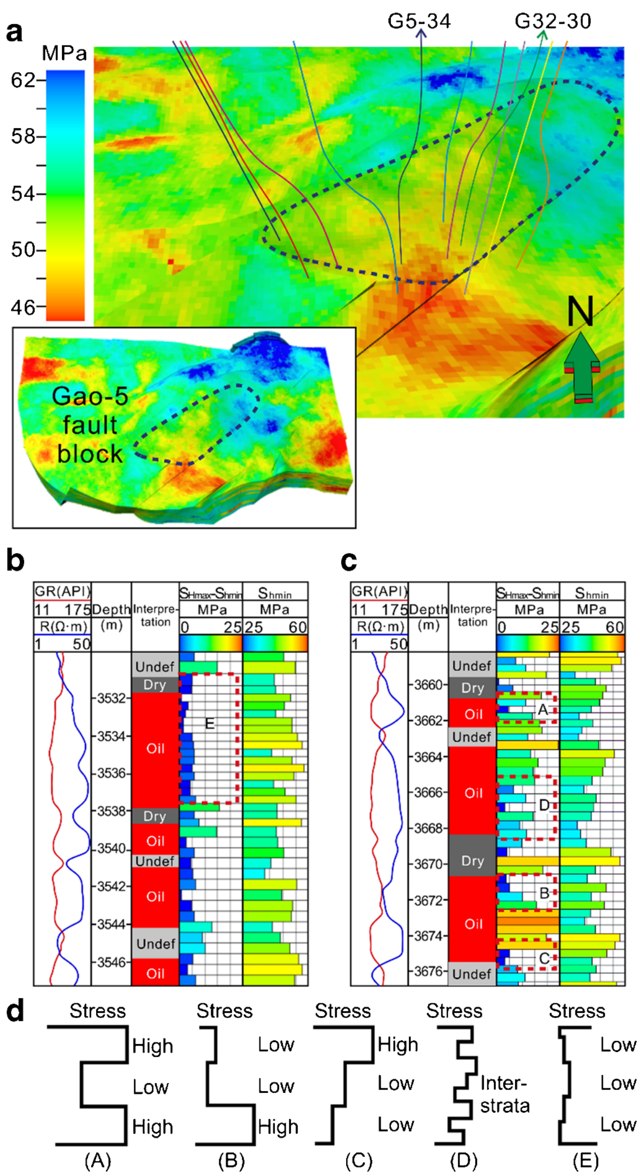

Fig. 11 Gao-5 fault block: in situ stress characteristics and profile types. **a** 3D distribution of S_{hmin} for GO-NA and Gao-5 fault block. **b** In situ stress profile of well G5-34. **c** In situ stress profile of well G32-30. **d** In situ stress profile types identified from GO-NA wells

Analysis of inter-strata in situ stress

Inter-strata in situ stress affects the height and direction in which fractures extend and expand, which is important in reservoir modeling. The combined Petrel and ANSYS modeling techniques allows the stress field predicted by numerical simulation to be used as a form of geological information for input into the 3D geological model. In turn, the characteristics of the stress field profile could be presented in detail in the Petrel grid (Fig. 11a–c).

The field profiles show great variation in the magnitude of in situ stress, with significant inter-strata differences. This is attributed to the quantitative relationship between rock mechanics parameters (especially Young's elastic modulus) and in situ stress magnitudes. Such inter-strata variations in in situ stress are directly related to the heterogeneity of the reservoir's rock mechanics parameters (Yan 2007).

Horizontal differential stress is the key factor controlling volumetric fracturing. A complex network of seams is easily formed when differential stress is small; otherwise, unidirectional fracturing will form parallel to S_{Hmax}. On the other hand, potential extensions of fracture height and length are mainly controlled by the distribution of the minimum principal stress above the fractured sections of the layer (Dong et al. 2005), and by S_{Hmax} orientation (Zhang et al. 2016), respectively.

The GO-NA was divided into five types of typical stress profile (types A–E; Fig. 11d), all of which were present in the in situ stress profiles of wells G5-34 and G32-30. As shown in Fig. 11b and c, the stress distribution pattern for type A is "high–low–high," meaning that fracturing operations in this area would be limited by the high differential stress (usually > 5 MPa) between the upper and lower strata. The possibility of the fracturing seam passing through the layer is small, thereby restricting the scale of the operation. For type B, the distribution pattern is "low–low–high." The horizontal differential stress of the upper layer should be within 4 MPa, whereas that of the lower layer is larger, meaning that upward fracture extensions readily occur. Under this scenario, all well sections with lower stress differences will be fractured. Thus, the volume of fluid injected and the scale of the operation must be carefully considered.

The type C distribution pattern is “high–low–low.” The horizontal differential stresses of the layers above and below are large and small, respectively, such that fractures tend to extend downward. Type D has an inter-strata distribution pattern, with the horizontal differential stress within the range of the well section being small. Nevertheless, variations exist, such that it is possible for the fracturing seam to extend either upward and/or downward, while the direction of extension may also change. The distribution pattern for type E is “low–low–low.” The horizontal differential stress within the well section is small and uniform, thereby readily facilitating extension of the fracturing seam both upward and downward. At the same time, complex networks of seams are likely to form, which provide ideal in situ stress conditions for fracturing operations.

Therefore, the distribution of inter-strata in situ stress must be clearly understood during fracturing operations, so that inter-strata fracture extensions can be predicted. Otherwise, sand blockages are likely to occur, resulting in suspension or even failure of fracturing operations. Furthermore, mud losses and other problems are associated with over- and under-pressurized boreholes. Accurate assessment of the possible heights and lengths of fracture extensions enables rational planning of the scale of operation and deployment of the well network, thereby improving the outcomes of reservoir reconstruction.

Conclusion

In this study, borehole breakouts and acoustic emissions (AE) were used to determine the orientation and magnitude of in situ stress in the Gaoshangpu Oilfield northern area, China. Several established approaches are available for measuring in situ stress, but each has particular shortcomings that may negatively affect the accuracy of the results. The modeling technique proposed here taps the advantages of both Petrel and ANSYS software to facilitate the construction of 3D models and heterogeneous rock mechanics fields. These improve the accuracy of simulated results, especially in terms of the clear presentation of inter-strata, in situ stress characteristics. The research results have been successfully applied for oil and gas exploitation by the PetroChina Jidong Oilfield Company. This technique was demonstrated as suitable for comprehensive prediction of the 3D distribution of in situ stress in a heterogeneous reservoir located within complex fault blocks. However, prediction of in situ stresses could be improved by considering fluid and temperature factors, and by modeling the dynamic in situ stress field during development of an oil and gas field.

The following conclusions were made:

i. The in situ stress field of the GO-NA can be predicted by considering spatial variations in mechanical parameters, and the morphology and occurrence of faults.
ii. Simulation results show that the overall orientation of maximum horizontal stress in the GO-AN is ENE–WSW, and is of lower magnitude in the west than the east.
iii. In situ stress magnitudes are discrete along surfaces and in profile, and is of the Ia-type, where: $S_V > S_{Hmax} > S_{hmin}$, and $S_{hmin} > 0$.
iv. Heterogeneity of the principal stress gradually decreases with increasing depth; inter-strata variations in in situ stress are significant and follow five profile types: high–low–high, low–low–high, high–low–low, inter-strata, and low–low–low.
v. Faults cause the greatest variations in the stress fields of reservoirs located within complex fault blocks, and can significantly affect the magnitudes and orientations of the in situ stress fields. The boundary faults of Gao-5 fault block significantly influence in situ stress in the GO-NA, causing deflection of stress orientation and reductions in stress magnitude. Next in importance are rock mechanics parameters, which significantly affect the magnitudes but not orientation of stresses. There is a high linear correlation between burial depth and in situ stress magnitude. Therefore, the critical prerequisites for studying the stress fields of regions with complex fault blocks include the characterization of faults, and construction of the heterogeneous rock mechanics field.

Funding information This research was jointly supported by the National Natural Science Foundation of China (41572124), National Science and Technology Major Project of the Ministry of Science and Technology of China (2016ZX05014002-006 and 2016ZX05047-003), and Independent Innovation Research Program of the CUP(H) (17CX05010 and 17CX06039). The funding source does not have any involvement in study design; in the collection, analysis, and interpretation of data; in the writing of the report; and in the decision to submit the article for publication.

References

Anderson EM (1951) The dynamics of faulting and dyke formation with applications to Britain, second edn. Oliver, Edinburgh, p 206

Bell JS (1996) Petro geoscience 2. In situ stresses in sedimentary rocks (part 2): applications of stress measurements. Geosci Can 23(3): 135–153

Bell JS (2006) In-situ stress and coal bed methane potential in Western Canada. Bull Can Petrol Geol 54:197–220

Bell JS, Gough DI (1979) Northeast-southwest compressive stress in Alberta: evidence from oil wells. Earth Planet Sci Lett 45:475–482

Binh NTT, Tokunaga T, Son HP, Binh MV (2007) Present-day stress and pore pressure fields in the Cuu Long and Nam Con Son Basins, offshore Vietnam. Mar Pet Geol 24:607–615

Brooke-Barnett S, Flottmann T, Paul PK, Busetti S, Hennings P, Reid R, Rosenbaum G (2015) Influence of basement structures on in situ stresses over the Surat Basin, southeast Queensland. J Geophys Res Solid Earth 120:4946–4965

Brown ET, Hoek E (1978) Trends in relationships between measured in-situ stresses and depth. Int J Rock Mech Min Sci Geomech Abstr 15: 211–215

Cao CJ 2005 Tectonic stress field analysis and application in the northwest Sichuan Basin. PhD dissertation, Graduate School of Chinese Academy of Geological Sciences, Beijing

Chen H, Wang XM, Zhao LX (2009a) Study of inversion for third order elastic constants and in-situ stress by multifrequency dispersion of cross dipole sonic logging. Chin J Geophys 52:1663–1674

Chen M, Yan Z, Yan J, Liangchuan LI (2009b) Experimental study of influence of loading rate on Kaiser effect of different lithological rocks. Chin J Rock Mech Eng 28:2599–2604

Dai JS (2002) Structural analysis of oil province. Petroleum University Press, Dongying, pp 167–188

Dai JS, Wang XT, Zong-Zhen JI, Xiao-Ming MA, Feng ZD, Zhang XG (2011) Structural stress field of Funing sedimentary period and its control on faults in the east of south fault terrace in Gaoyou Sag. J China Univ Pet 35(2):1–5+19

Dai JS, Zou J, Zhao XZ, Lu LF, Sun ZH (2014) Fault characteristics interpretation of Ek-E_{s4} sedimentary period in Hexiwu tectonic belt through stress field simulation. Nat Gas Geosci 25(10):1529–1536

Dai JS, Liu JS, Yang HM, Zhang Y, Wang BF, Zhou JB (2016) Numerical simulation of stress field of Fu-2 member in Tongcheng fault zone and development suggestions. J China Univ Pet Ed Nat Sci 40:1–9

Ding WL, Fan TL, Huang XB, Li CY (2011) Upper Ordovician paleo tectonic stress field simulating and fracture distribution forecasting in Tazhong area of Tarim Basin, Xinjiang, China. Geol Bull China 30(4):588–594

Ding W, Zeng W, Wang R, Jiu K, Wang Z, Sun Y, Wang X (2016) Method and application of tectonic stress field simulation and fracture distribution prediction in shale reservoir. Earth Sci Front 23(2): 63–74. https://doi.org/10.13745/j.esf.2016.02.008

Dong JH, Liu P, Wang W (2005) Application of in situ stress profile to hydraulic fracturing. J Northeast Pet Univ 29:40–42

Dong YX, Xiao L, Zhou HM, Wang CZ, Zheng JP (2010) The tertiary evolution of the prolific Nanpu Sag of Bohai Bay Basin, China: Constraints from volcanic records and tectono–stratigraphic sequences. GSA Bull 122:609–626

Engelder T (1993) Stress regimes in the lithosphere. Princeton University Press, Princeton, pp 23–30

Fan YR, Wei ZT, Chen XL (2009) Study on formation stress calculation and its influential factors based on logging data. Well Logging Technol 33:415–420

Farrell NJC, Healy D, Taylor CW (2014) Anisotropy of permeability in faulted porous sandstones. J Struct Geol 63:50–67

Finkbeiner T, Zoback M, Flemings P, Stump B (2001) Stress, pore pressure, and dynamically constrained hydrocarbon columns in the South Eugene Island 330 field, northern Gulf of Mexico. AAPG Bull 85:1007–1031

Gong ZS (1997) Giant offshore oil and gas fields in China. Petroleum Industry Press, Beijing (in Chinese)

Haghi AH, Kharrat R, Asef MR, Rezazadegan H (2013) Present-day stress of the central Persian Gulf: implications for drilling and well performance. Tectonophysics 608:1429–1441

He SM, Wang W, Shen H, Tang M, Liang HJ, Lu JA (2015) Factors influencing wellbore stability during underbalanced drilling of horizontal wells when fluid seepage is considered. J Nat Gas Sci Eng 23:80–89

Hoda D, Morteza NT, Amin S, Afshin T (2015) Geo-mechanical modeling and selection of suitable layer for hydraulic fracturing operation in an oil reservoir (south west of Iran). J Afr Earth Sci 111:409–420

Holcomb DJ (1993) Observations of the Kaiser effect under multiaxial stress states: implications for its use in determining in situ stress. Geophys Res Lett 20:2119–2122

Hudson JA, Cooling CM (1988) In situ rock stresses and their measurement in the U.K.—Part I. The current state of knowledge. Int J Rock Mech Min Sci Geomech Abstr 25:363–370

Ju W, Sun WF (2016) Tectonic fractures in the Lower Cretaceous Xiagou Formation of Qingxi Oilfield, Jiuxi Basin, NW China. Part two: Numerical simulation of tectonic stress field and prediction of tectonic fractures. J Pet Sci Eng 146:626–636

Ju W, Shen J, Qin Y, Meng S, Wu C, Shen Y et al (2017) In-situ stress state in the Linxing region, eastern Ordos Basin, China: implications for unconventional gas exploration and production. Mar Pet Geol 86:67–78

Kang H, Zhang X, Si L, Wu Y, Gao F (2010) In-situ stress measurements and stress distribution characteristics in underground coal mines in China. Eng Geol 116:333–345

Kingdon A, Fellgett MW, Williams JDO (2016) Use of borehole imaging to improve understanding of the in-situ stress orientation of Central and Northern England and its implications for unconventional hydrocarbon resources. Mar Pet Geol 73:1–20

Lehtonen A, Cosgrove JW, Hudson JA et al (2012) An examination of in situ, rock stress estimation using the Kaiser effect. Eng Geol 124: 24–37

Lei G, Dai J, Yujie MA, Wang K, Yang X, Qing LI (2015) Numerical simulation of the current stress field and reservoir fracture in Keshen 3D area of Kuqa Depression. Pet Geol Oilfield Dev Daqing 34(1): 18–23

Li LI, Zou Z, Zhang Q (2011a) Current situation of the study on Kaiser effect of rock acoustic emission in in-situ stress measurement. Coal Geol Explor 39(1):41–392

Li SB, Dou TW, Dong DR, Zhang HY, Wang M, Liu TE (2011b) Stress state of bottom-hole rocks in underbalanced drilling. Acta Pet Sin 32:329–334

Li Y, Tang DZ, Xu H, Yu TX (2014) In-situ stress distribution and its implication on coalbed methane development in Liulin area, eastern Ordos Basin. China J Pet Sci Eng 122:488–496

Liu QJ, Yan XZ, Yang XJ (2009) Application of optimization back-analysis method in reservoir stress and fracture study. Pet Drill Tech 37:26–31

Liu R, Liu JZ, Zhu WL, Hao F, Xie YH, Wang ZF, Wang LF (2016) In situ stress analysis in the Yinggehai Basin, northwestern South China Sea: implication for the pore pressure-stress coupling process. Mar Pet Geol 77:341–352

Lommatzsch M, Exner U, Gier S, Grasemann B (2015) Dilatant shear band formation and diagenesis in calcareous, arkosic sandstones, Vienna Basin (Austria). Mar Pet Geol 62:144–160

Lu SK, Wang D, Li YK, Meng XJ, Hu XY, Chen SW (2015) Research on three-dimensional mechanical parameters' distribution of the tight sandstone reservoirs in Daniudi Gasfield. Nat Gas Geosci 26:1844–1850

Mann P, Hempton MR, Bradley DC, Burke K (1983) Development of pull-apart basins. J Geol 91(5):529–554

Mizuta Y, Sano O, Ogino S, Katoh H (1987) Three dimensional stress determination by hydraulic fracturing for underground excavation design. Int J Rock Mech Min Sci Geomech Abstr 24(1):15–29

Nelson PH (2009) Pore- throat sizes in sandstones, tight sandstones, and shales. AAPG Bull 93(3):329–340

Plumb RA, Hickman SH (1985) Stress-induced borehole elongation: a comparison between the four-arm dipmeter and the borehole televiewer in the Auburn Geothermal Well. J Geophys Res 90:5513–5521

Rajabi M, Sherkati S, Bohloli B, Tingay M (2010) Subsurface fracture analysis and determination of in-situ stress direction using FMI logs: an example from the Santonian carbonates (Ilam Formation) in the Abadan Plain, Iran. Tectonophysics 492:192–200

Savage WZ, Swolfs HS, Amadei B (1992) On the state of stress in the near-surface of the earth's crust. Pure Appl Geophys 138:207–228

Sibson R (1994) Crustal stress, faulting and fluid flow. Geol Soci of London, Special Publication, London 78:69–84

Tian YP, Liu X, Li X, Wei M (2011) Finite element method of 3-D numerical simulation on tectonic stress field. Earth Sci J China Univ Geosci 36:375–380

Tingay M, Hills RR, Morley CK, King RC, Swarbrick RE, Damit AR (2009) Present-day stress and neotectonics of Brunei: implications for petroleum exploration and production. AAPG Bull 93(1):75–100

Tingay MRP, Morley CK, Hillis RR, Meyer J (2010) Present-day stress orientation in Thailand's basins. J Struct Geol 32:235–248

Wan JB, Bai ST, Guo XK, Huang Y, Li XN, Mao T (2015) Productivity prediction methods of low porosity and permeability in deep reservoir in Nanpu Sag. Well Logging Technol 39:373–378

Wang K 2014 Quantitative description of fracture of clastic reservoir in gram gas field. PhD dissertation, China University of Petroleum, Tsingtao

Wang BF, Dai JS, Cheng RH, Yan P, Wang YH (2007) Present ground stress in Dina gas field. Xinjiang Pet Geol 28(4):471–470

Wang XJ, Peng SM, Lv BX, Ma JY (2008) Researching earth stress field using cross dipole acoustic logging technology. J China Univ Pet Nat Sci Ed 32:42–46

Wang K, Dai JS, Feng JW, Wang JP, Li Q (2014) Research on reservoir rock mechanical parameters of Keshen foreland thrust belt in Tarim Basin. J China Univ Pet Ed Nat Sci 38:25–33

Wang S, Dai J, Fu X, Wang Y, Chen G, Xu F (2016) Numerical simulation research on current stress of Es3 of the 5th block of Bonan oilfield and analysis of its influence factors. Pet Geol Recover Efficiency 23(3):26–32

Xie RC, Zhou W, Tao Y, Wang SZ, Yao J, Deng H (2008) Application of finite element analysis in the simulation of the in-situ stress field. Pet Drill Technol 36:60–63

Xu K (2019) Current in-situ stress of Gaoshangpu reservoir, Nanpu Sag, Bohai Bay Basin, China. PhD dissertation, China University of Petroleum, Qingdao

Xu K, Dai J, Shang L, Fang L, Feng J, Du H (2019) Characteristics and influencing factors of in-situ stress of Nanpu sag, Bohai Bay basin, China. J China Univ Min Technol 48(3):500–513

Yan P 2007 The earth stress calculation using well logging data and its applied research in piedmont structure: University of Petroleum, M.E. Thesis, Beijing

Yang XQ, Shi XB, Xu HH (2012) Numerical modeling of the current tectonic stress field. Chin J Geophys Taiwan Strait Adjacent Regions 55:2307–2318

Yu X, Hou GT, Li Y, Lei GL, Neng Y, Wei HX, Zheng CF, Zhou L (2016) Quantitative prediction of tectonic fractures of lower Jurassic Ahe formation sandstones in Dibei gasfield. Earth Sci Front 23:240–252

Zang A, Stephansson O (2009) Stress field of the Earth's crust. Springer Netherlands, Berlin, pp 131–192

Zeng LB, Su H, Tang XM, Peng YM, Gong L (2013) Fractured tight sandstone oil and gas reservoirs: a new play type in the Dongou depression, Bohai Bay Basin, China. AAPG Bull 97(3): 363–377

Zhang CM 2010 Tectono-sedimentary analysis of Nanpu Sag in the Bohaiwan Basin. PhD dissertation, China University of Geosciences, Beijing

Zhang ZY, Wu ML, Chen QC, Liao CT, Feng CT (2012) Review of in-situ stress measurement methods. J Henan Polytechnic Univ (Ed Nat Sci) 31:305–310

Zhang ZQ, Zhang YM, Bu XQ, Liang YH, Zhang EY (2016) A study of in-situ stress direction change during waterflooding in the low permeability reservoirs. J Peking Univ (Ed Nat Sci) 52: 861–870

Zhao K, Yan DQ, Zhong CH, Zhi XY, Wang XJ, Xiong XQ (2012) Comprehensive analysis method and experimental verification for in-situ stress measurement by acoustic emission tests. Chin J Geotechn Eng 34(8):1403–1411

Zhu CH, Wang WF, Wang QZ, Li YK (2016) Numerical simulation of structural strain for turbidite sands reservoirs of low permeability. J Jilin Univ (Earth Sci Ed) 46:1580–1588

Zoback MD (2007) Reservoir Geomechanics. Cambridge University Press, Cambridge, p 449

Zoback MD, Barton CA, Brudy M, Castillo DA, Finkbeiner T, Grollimund BR, Moos DB, Peska P, Ward CD, Wiprut DJ (2003) Determination of stress orientation and magnitude in deep wells. Int J Rock Mech Min Sci 40:1049–1076